Biomaterials Science

ROYAL SOCIETY OF CHEMISTRY

PAPER

View Article Online
View Journal | View Issue

Cite this: *Biomater. Sci.*, 2025, **13**, 5512

Real-time monitoring of mitochondrial temperature and calcium spikes using fluorescent organic probes

Mengnan Sun,[a] Bo Chen *[b,c] and Aiguo Wu *[a,b,c]

Received 4th May 2025,
Accepted 12th August 2025

DOI: 10.1039/d5bm00691k

rsc.li/biomaterials-science

Astrocytes, the abundant glial cells, maintain cerebral homeostasis and cognitive functions through calcium signalling – a regulatory pathway that is frequently altered in brain disease. Mitochondria serve as thermal hubs in living systems, generating metabolic heat during respiratory substrate oxidation and ATP synthesis. Crucially, mitochondrial temperature variations directly reflect metabolic status, as impaired ATP production induces thermodynamic shifts. Here, we utilized a fluorescent thermometer probe MTY for *in vitro* determination and visualization of intracellular mitochondrial temperatures at the single-cell level. Through precisely controlled thermal modulation of fixed, living, and laser-stimulated astrocytes, we established a platform extendable to MCF-7 and Panc02 cell lines. The methodology enabled real-time tracking of near-infrared-induced thermal perturbations and FCCP-mediated uncoupling effects. Spinning-disk confocal microscopy revealed synchronized mitochondrial thermogenesis and calcium transients, with thermal/laser stimulation inducing 2–4-fold greater calcium spiking *versus* controls. Mechanistic analysis suggested this response was likely mediated through TRPV4 channel-mediated extracellular Ca^{2+} influx and/or intracellular calcium release from mitochondrial and endoplasmic reticulum stores.

1 Introduction

Temperature serves as a critical regulator of biological processes in living organisms, governing the chemical reaction rates in various compartments,[1,2] modulating protein dynamics,[3] and influencing gene transcription.[4] The morphology of cells tends to shrink at both higher and lower temperatures, indicating that the cells are highly sensitive to temperature fluctuations. This central role underscores the importance of precisely measuring and controlling the intracellular temperature at subcellular resolutions to elucidate how thermal dynamics intersect with biological functions.

Mitochondria, often celebrated as the cell's "powerhouses", are indispensable components of eukaryotic cells, best known for their role in adenosine triphosphate (ATP) synthesis. They perform diverse cellular functions beyond energy production.[5] Through oxidative phosphorylation and other biochemical processes, mitochondria generate substantial heat, playing a central role in maintaining temperature homeostasis within cells.[6] The heat distribution is influenced by cellular structures like cytoplasmic barriers and membranes that restrict thermal exchange, resulting in distinct temperature microenvironments within mitochondria compared to the normal broader cell.[7] Cancer cells and inflammatory cells show enhanced mitochondrial metabolism, leading to increased cellular temperatures.[8] Counterintuitively, mitochondria can sustain a physiological temperature of nearly 50 °C without causing damage to the cells.[9] Therefore, it is very meaningful to obtain a deeper understanding of the local intracellular temperature as well as temperature changes during therapy and the effect on biological systems. Additionally, intracellular calcium ions (Ca^{2+}), among the most versatile signalling molecules critical for regulating secretory functions, enzyme activity, intracellular transport, membrane potential, and intercellular communication, exhibit dynamic fluctuations such as spontaneous oscillations or transient spiking.[10–12] Imaging studies of astrocytic Ca^{2+} dynamics have revealed that astrocytes enter a hyperactive state in numerous neurological diseases, including traumatic brain injury, epilepsy, and Alzheimer's disease (AD).[10,13] Mitochondria further play an important role in regulating the intracellular Ca^{2+} concentration by acting as local Ca^{2+} buffers.[14] Therefore, elucidating the interplay between intracellular temperature fluctuations and Ca^{2+} spiking patterns

[a]*Cixi Biomedical Research Institute, Wenzhou Medical University, Ningbo 315302, China. E-mail: aiguo@nimte.ac.cn*
[b]*Laboratory of Advanced Theranostic Materials and Technology, Ningbo Institute of Materials Technology and Engineering, Chinese Academy of Sciences, Ningbo 315201, China. E-mail: chenbo@nimte.ac.cn*
[c]*Ningbo Cixi Institute of Biomedical Engineering, Ningbo 315300, China*

could advance our understanding of the mechanisms underlying these neurological diseases.

In recent years, the development of fluorescent probes as temperature sensors, often referred to as "fluorescent thermometers", has garnered significant attention for use in targeted biological environments. These probes include a wide variety of materials, including organic small-molecule dyes, nanodiamonds, polymeric nanoparticles, and fluorescent proteins.[15–17] Owing to their exceptional localization performance, good membrane permeability, and remarkable biocompatibility, organic thermometers are highly suitable for biological research applications.[8,18–22] Chang *et al.* developed Mito Thermo Yellow (MTY), a mitochondria-targeted probe capable of measuring intracellular temperature with a sensitivity of 2.5–2.8% per °C in 3T3, HeLa, Chang, and mouse embryonic stem cells. MTY is built on the rosamine backbone, inheriting its inherent mitochondrial localization propensity and temperature-responsive properties, which are likely mediated by the rotational flexibility of its piperidine substituent.[18] Zhu *et al.* developed TRN, a near-infrared small-molecule probe designed to track mitochondrial temperature fluctuations in Huh7 carcinoma cells.[19] Takeoka *et al.* engineered Mito-RTP, a ratiometric fluorescent probe that localizes in mitochondria and enables temperature visualization in HeLa cells with a thermal sensitivity of −2.72% per °C.[20] To reduce variation in the inner-membrane potential of mitochondria, Xiao *et al.* developed Mito-TEM, a fixable fluorescent thermometer that allows for the visualization and quantification of mitochondrial temperature distribution through grayscale imaging, and Mito-TEM 2.0, a ratiometric probe that can visualize the mitochondrial temperature in live MCF-7 cells and zebrafish during various inflammation processes.[8,21] Bai *et al.* developed RhBIV, a thermosensitive fluorogenic probe derived from rhodamine B (RhB), which demonstrates a temperature-dependent response in the mitochondria of HepG2 cells with a sensitivity of 3.92% per °C.[22] For fluorescence-based thermometers, however, photobleaching remains a critical consideration, particularly in applications requiring prolonged tracking or sensing. To address this issue, spinning-disk confocal microscopy, with its array of hundreds of spirally arranged pinholes on a rapidly rotating disk and high-speed camera acquisition, provides an effective way to minimize photobleaching and phototoxicity, making it well-suited for prolonged imaging and sensitive measurements.

In this study, the intracellular temperature was monitored using the fluorescent thermometer probe MTY. Thermal stimuli were applied *via* three distinct methods: using a stage-top incubator, FCCP chemical stimulation, and near-infrared (NIR) laser stimulation. This approach enabled precise control and measurement of temperature changes within cellular environments. We then utilized a spinning-disk confocal microscope to achieve simultaneous imaging of changes in intracellular temperature and calcium spikes, the latter of which reflect neural activity. This was accomplished using the green fluorescent calcium indicator Fluo-4 AM and the red fluorescent temperature-sensitive probe MTY. A major strength of this dual-imaging approach is the minimal spectral overlap between the two dyes, which enables accurate and real-time measurement of both parameters concurrently. This system provides a powerful tool for capturing dynamic intracellular processes with high precision.

2 Experimental

2.1 Chemicals and materials

Fluo-4 AM (Ultrapure Grade) was purchased from AAT Bioquest (Pleasanton, CA, USA). Mito Thermo Yellow (MTY, λ_{ex} = 542 nm, λ_{em} = 564 nm) was obtained from Senpro Co. (Pohang, Republic of Korea). Carbonyl cyanide 4-(trifluoromethoxy) phenylhydrazone (FCCP), bovine serum albumin (BSA) and fetal bovine serum (FBS) were bought from Sigma-Aldrich (St Louis, MO, USA). PKmito DEEP Red (λ_{ex} = 644 nm, λ_{em} = 670 nm) was obtained from GenVivo Biotech (Nanjing, China). High-glucose Dulbecco's modified Eagle's medium (DMEM), phosphate-buffered saline (PBS, pH 7.4), Hank's balanced salt solution (HBSS) and penicillin/streptomycin were purchased from Procell Co. (Wuhan, China). HC-067047 and 4α-phorbol-12,13-didecanoate (4α-PDD) were obtained from MedChemExpress (Shanghai, China). Transient receptor potential vanilloid 4 (TRPV4) antibody (DF8624) and Fluor488-conjugated goat anti-rabbit IgG (H + L) antibody were purchased from Affinity Biosciences (Jiangsu, China). All chemicals were purchased from commercial suppliers and used as received without additional purification.

2.2 Cell culture and fluorescence imaging

The C8-D1A astrocyte cell line, originating from the cerebral cortex of an 8-day-old C57BL/6 mouse, is commonly used in neurobiological research due to its pronounced astrocytic properties. The Panc02 cell line, a commonly used murine model for studying pancreatic ductal adenocarcinoma, along with the C8-D1A cells, was obtained from Pricella Biotech (Wuhan, China). MCF-7 human breast carcinoma cells were obtained from the Institute of Basic Sciences (IBMS) of the Chinese Academy of Medical Sciences (CAMS). All these cell types are cultured in high-glucose DEMEM enriched with 10% fetal bovine serum (FBS) and penicillin (0.1 U mL^{-1})– streptomycin (0.1 mg mL^{-1}) at 37 °C in an incubator equipped with a CO_2 tank to maintain conditions of 37 ± 0.5 °C, 5% ± 0.1% CO_2, and 95–100% humidity.

Fluorescence spectra and intensity measurements were performed using a fluorescence spectrophotometer (FL-55, PerkinElmer, USA) equipped with a temperature controller. Cell viability and cytotoxicity assays were conducted using a multimode plate reader (Victor Nivo, PerkinElmer, USA).

2.3 Live cell calcium signaling and drug treatment

To study the intracellular calcium signaling, the astrocytes were loaded with 0.25 μM Fluo-4 AM in phenol red-free DMEM for 30 min at 37 °C, rinsed three times with DMEM, then immersed in an artificial cerebrospinal fluid (HBSS: 125 mM NaCl, 3 mM

KCl, 10 mM glucose, 26 mM $NaHCO_3$, 1.1 mM NaH_2PO_4, 2 mM $CaCl_2$, 1 mM $MgSO_4$; pH adjusted to 7.4) and imaged. Fluorescence signals that represent calcium dynamics were monitored in real time at 10 s intervals for a period of 10–20 min.

HC-067047 was pre-incubated at a concentration of 1 μM for 24 h. The agonist experiment was divided into three groups: a room temperature (RT) control group, a 4α-PDD treatment group, and a 4α-PDD treatment with high temperature (HT) group. In the 4α-PDD treatment group, 4α-PDD was added at a concentration of 1 μM prior to testing. Quantitative analysis of treatment effects was performed using a flow cytometer (BD LSRFortessa, USA).

2.4 Immunofluorescence staining

Cultured astrocytes were fixed with 4% paraformaldehyde (room temperature, 15 min), followed by three PBS washes (5 min each). The cells were permeabilized with 0.2% Triton X-100 (5 min) and nonspecific binding sites were blocked with 5% BSA (1 h). Subsequently, the cells were incubated for 1 h at room temperature with a primary TRPV4 monoclonal antibody (dilution ratio: 1 : 250), washed three times with PBS, and incubated for 1 h with a secondary goat anti-rabbit IgG (H + L) antibody conjugated to Fluor488 (1 : 500). Control experiments omitted the primary antibody incubation while maintaining all other procedural steps.

2.5 Imaging platform construction

The images were captured using an Andor Dragonfly spinning-disk confocal microscope equipped with a Nikon CFI plan lambda D 20×/0.80 N.A. objective. A scientific complementary metal–oxide semiconductor (sCMOS) camera (Andor Sona 4.2B-11) was utilized alongside the 488 nm (Fluo-4 AM) and 568 nm (mitochondrial) lines from the Andor Integrated Laser Engine (ILE) system, combined with the spinning-disc confocal scan head (Andor Dragonfly 202). Specifically, images were acquired with laser powers of 2–4% for both the 488 nm and 561 nm lasers, with exposure times ranging from 10 to 20 ms; the acquisition was performed using Fusion software (**https://andor.oxinst.com/products/dragonfly-confocal-microscope-system#fusion**). Following acquisition, the images were processed using FIJI: ImageJ (**https://imagej.net/software/fiji/downloads**) or Imaris 10.2 (Oxford Instruments, UK) for quantitative data analysis and channel merging. Data were primarily expressed as fluorescence intensity (F) or the calcium dynamic change in fluorescence ($\Delta F = F - F_0$), normalized to the baseline fluorescence intensity (F_0) prior to stimulation. A stage-top incubator (Tokai Hit, Japan) was used to control the temperature.

The study of the effect of local heating on living cells induced by an NIR laser was carried out using a custom-designed system (Fig. S1). The system incorporated three lasers: a 1064 nm NIR laser (Beijing Honglan Optoelectronics Technology Co., Ltd; model VCL-1064 nm M0-10W) to heat the cells and surrounding medium, and two additional lasers (488 nm and 561 nm) to excite the Fluo-4 AM calcium indicator dye, enabling visualization of intracellular Ca^{2+} dynamics and concurrent monitoring of MTY fluorescence, respectively. The NIR laser beam was delivered *via* an optical fiber coupled to a diffuser, homogenizing the beam profile before positioning it above the Petri dishes for uniform heating, and visible light was coupled before laser stimulation for well alignment of the laser beam. The 488 nm and 561 nm excitation lasers were directed through a 20× or 40× objective lens to illuminate the coverslip surface from the bottom, ensuring precise fluorescence imaging. A fiber temperature sensor was used to monitor the temperature in the cell culture in real time throughout the process.

2.6 Statistical analysis

The data are presented as mean ± standard deviation (SD). All cells were analyzed from independent experiments, each repeated at least three times. Statistical analysis was conducted using OriginPro software student version (OriginLab, Northampton, MA). Differences were assessed using Student's t-test, with statistical significance set at $^{*}p < 0.05$, $^{**}p < 0.01$, and $^{***}p < 0.001$.

3 Results and discussion

3.1 Temperature sensitivity evaluation of MTY in PBS

To investigate the temperature-dependent behavior of MTY, its fluorescence was measured in PBS using a fluorescence spectrometer equipped with a temperature controller. As shown in Fig. 1a and b, MTY exhibits a gradual decrease in fluorescence intensity as the temperature rises from 25 to 45 °C, suggesting its potential utility as a fluorescent temperature probe.

3.2 Cell viability and cytotoxicity evaluation of MTY

The Cell Counting Kit-8 (CCK-8) assay is a widely used method for evaluating cell viability and cytotoxicity. The astrocyte cells were incubated with various concentrations of MTY in a 96-well plate for 24 h and then their cell viability was tested according to the CCK-8 protocol. As demonstrated in Fig. 1c, the cell viability of astrocyte cells remains nearly 80% even at the higher concentration of 300 nM MTY, which is greater than the concentration used in this study. This indicates that MTY exhibits low cytotoxicity and holds significant potential for real applications in live cell imaging and labelling.

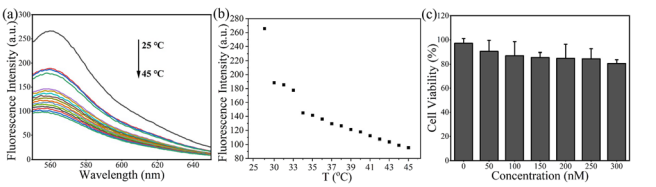

Fig. 1 Fluorescence titration and cell viability. (a) Fluorescence spectra of MTY (10 μM) as functions of temperature changes. (b) Plot of fluorescence intensity at 560 nm *vs.* temperature. (c) Cell viability test with different concentrations of MTY.

3.3 Mitochondrial localization evaluation of MTY

The ability of MTY to target mitochondria was evaluated through a colocalization experiment in astrocyte cells. The commercial PKMDR which served as a better alternative to traditional mitochondria markers like MitoTracker and MTY were chosen to stain astrocyte cells simultaneously in serum-free DMEM without phenol red.[23,24] As shown in Fig. 2, the fluorescence distribution of MTY (λ_{ex} = 561 nm) closely matched that of PKMDR (λ_{ex} = 640 nm) with a Pearson's colocalization coefficient of 0.962. This high coefficient demonstrates a strong colocalization between them. Consequently, MTY is specifically localized within the mitochondrial regions of astrocyte cells.

3.4 Mitochondrial-temperature sensitivity evaluation of MTY in fixed cells

As we know, the purpose of the paraformaldehyde fixation method is to maintain the structural stability of cells and prevent morphological alterations during subsequent experimental procedures. We first assessed whether the fluorescence intensity of MTY varied reversibly in response to heating and cooling in fixed cells. The cells were initially incubated with MTY, fixed with a 4% paraformaldehyde solution for 15 minutes, thoroughly washed several times with PBS, and then subjected to temperature control using a stage-top incubator. As shown in Fig. S2, the fluorescence intensity of MTY has almost no change or just exhibits minor fluctuations under constant room temperature conditions. In contrast, Fig. 3 demonstrates that the fluorescence intensity of MTY in astrocyte cells gradually decreased as the temperature rose from 21.33 to 34.52 °C, yielding a linear equation (y = $-0.01734x$ + 1.00882) with a correlation coefficient of 0.959. Conversely, fluorescence imaging confirmed a linear temperature dependence of MTY signal rise during gradual thermal decrease. Besides astrocytes, other cells such as MCF-7 and Panc02 cells also exhibited similar trends (Fig. S3 and Fig. S4), further validating MTY's reversible sensitivity to microenvironmental thermal changes under fixed-cell conditions, and could be widely used in other cell lines.

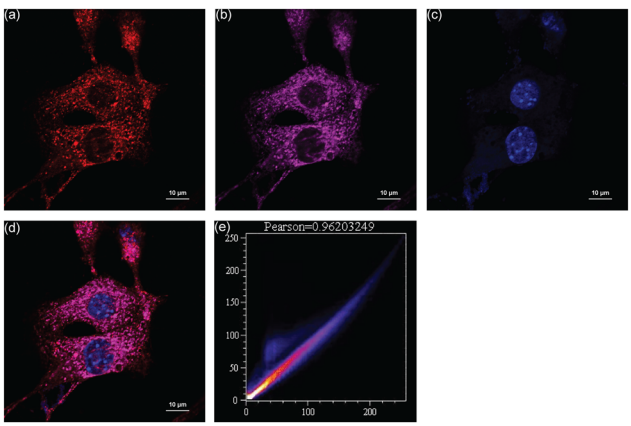

Fig. 2 Confocal images of astrocyte cells costained with MTY, PKMDR and Hoechst 33258. (a) MTY red channel. (b) PKMDR purple channel. (c) Nuclei blue channel. (d) Merge channel. (e) The colocalization scatterplot based on red and cyan pixel intensities of the image.

3.5 Mitochondrial-temperature sensitivity evaluation of MTY in living cells

Fluorescence imaging-based measurement of local mitochondrial temperature in living cells presents significant challenges, primarily due to dynamic fluctuations in the mitochondrial microenvironment (*e.g.*, pH, membrane potential, ion channel activity, and viscosity). Herein, the following experiments were carried out. First, MTY-stained astrocyte cells were incubated in culture media subjected to controlled external heating using a stage-top incubator, followed by real-time fluorescence imaging. As demonstrated in Fig. 4, the MTY fluorescence intensity exhibited a gradual decrease as the extracellular medium temperature rose from 20.51 to 34.20 °C. This trend was described using a linear equation (y = $-0.01331x$ + 1.01085) with a correlation coefficient of 0.97. This observation suggests that external heating induces a measurable elevation in mitochondrial temperature. This divergence likely reflects the intrinsic thermoregulatory capacity of living cells, which enables adaptive responses to external thermal perturbations in a short time. However, during the cooling period, the temperature declines very slowly, and the progressive shrinkage of cell morphology limits our ability to track the process over extended durations. Consequently, the cooling curve exhibits a less pronounced downward trend compared to that of fixed cells.

Second, FCCP, a known inhibitor of oxidative phosphorylation, disrupts ATP synthesis by transporting protons across the mitochondrial inner membrane,[25] thereby elevating mitochondrial temperature. In this experiment, astrocyte cells were prestained with MTY for 30 minutes, washed three times with PBS, incubated in phenol red-free DMEM and subsequently treated with 10 μM FCCP that was added directly to the culture medium. Fluorescence imaging was performed continuously over 30 minutes to track the correlation between the mitochondrial temperature dynamics and MTY's fluorescence intensity across individual astrocyte cells. As shown in Fig. 5 (detailed images are shown in Fig. S5), baseline fluorescence measurements (initial 5 minutes) revealed no significant changes, indicating stable intracellular temperatures prior to FCCP exposure. Subsequently, the FCCP introduction triggered a sharp decline in MTY fluorescence within 5 minutes, indicative of rapid mitochondrial heating, followed by a gradual signal recovery—a phenomenon likely attributable to cellular compensatory mechanisms. Notably, concurrent fiber thermometer measurements confirmed no detectable temperature changes in the extracellular medium, ruling out environmental thermal effects. Therefore, a distinct discrepancy between mitochondrial temperatures in living cells and the extracellular medium has been revealed. These findings also clearly demonstrate MTY's efficacy as a precise intracellular thermosensor, capable of monitoring subcellular thermal fluctuations without interference from external conditions.

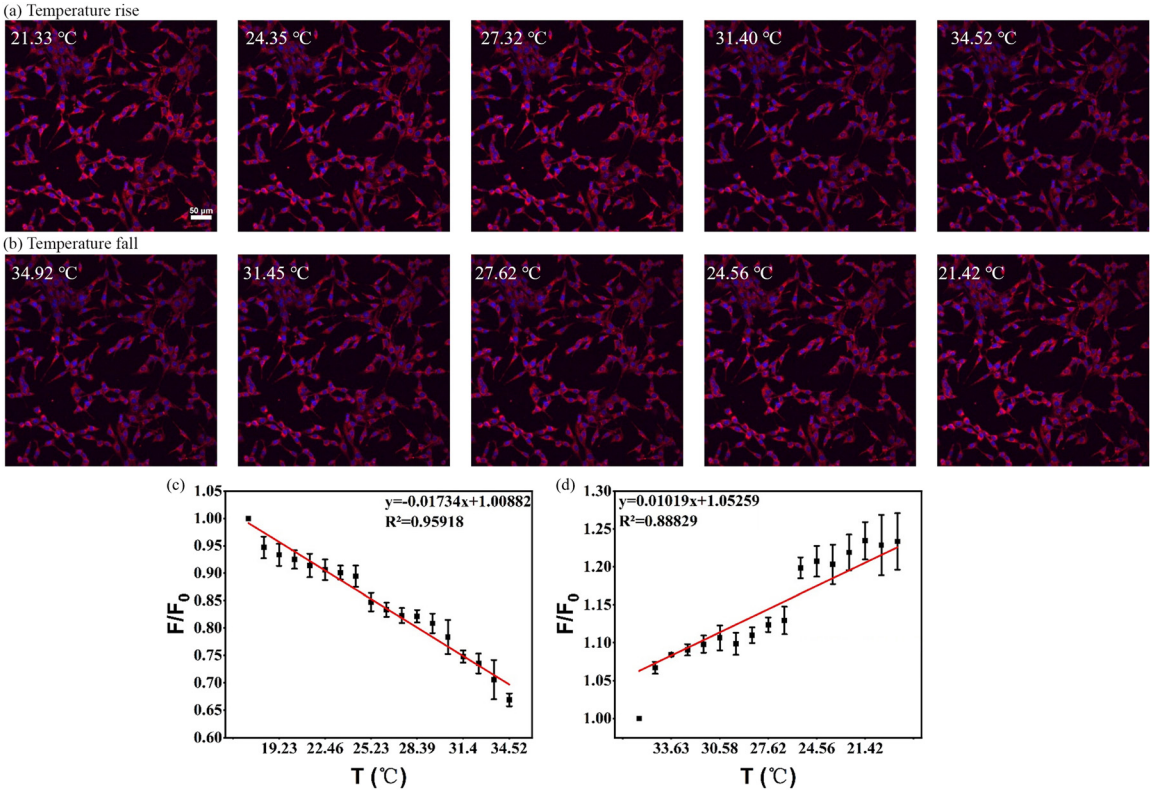

Fig. 3 Tracking changes in MTY fluorescence intensity through temperature changes in fixed astrocyte cells. (a) Time-lapse of MTY fluorescence intensity in astrocyte cells with increasing temperature. (b) Time-lapse of MTY fluorescence intensity in astrocyte cells with decreasing temperature. (c) Plot of MTY fluorescence intensity against increasing temperature in astrocyte cells. (d) Plot of MTY fluorescence intensity against decreasing temperature in astrocyte cells. Nuclei were counterstained with DAPI (blue) and imaged using a 20× objective lens.

3.6 Optimal condition evaluation of the infrared laser system

Thermal stimulation is one kind of non-invasive, optically induced thermal modulation. The mechanism underlying thermal modulation of neural activity is thought to involve a combination of temperature-induced changes in transmembrane capacitance and alterations in the conductance dynamics of certain ion channels. Usually, rapid heating is achieved through the exposure to NIR laser illumination; thus, this method is often named as infrared neuromodulation (INM).[26] In this study, a 1064 nm infrared laser was utilized for delivering non-invasive stimulation to enhance cellular activity. The laser emitted a collimated beam with a spot area of 9.62 cm^2, producing a power density of 0.208 W cm^{-2} at a 2.0 W output. Over a 20-minute irradiation period (1200 seconds), a total energy dose of 2400 J was delivered (2.0 W × 1200 s = 2400 J), equivalent to an energy density of 249.48 J cm^{-2}. To identify optimal experimental conditions, laser power and irradiation duration were systematically tested. As illustrated in Fig. S6, temperature elevation occurred more rapidly under high-power illumination and with smaller solution volumes. Therefore, the optimal conditions (2.0 W and 1.0 mL) were selected for late laser experiments.

The baseline temperature of the culture medium was recorded prior to laser irradiation and subsequently under predefined exposure parameters that included variations in laser intensity and irradiation time. Real-time temperature monitoring was conducted during laser stimulation using a thermistor-based measurement system. Experimental data revealed that elevated laser power levels (*e.g.* 2 W) produced significant temperature increases exceeding 8.0 °C, demonstrating a clear power-dependent thermal response. These observations indicate the occurrence of measurable thermal effects at higher energy densities.

3.7 Mitochondrial-temperature sensitivity evaluation of MTY in living cells using NIR laser stimulation

Fig. 6 reveals that under NIR laser stimulation the fluorescence intensity of MTY in living astrocyte cells gradually declined as the temperature increased from 23.69 to 32.43 °C. This trend was described using a linear equation ($y = -0.01709x + 0.9688$) with a correlation coefficient of 0.98. Conversely, fluorescence imaging showed a linear increase in the MTY signal as the temperature gradually decreased, indicating a clear temperature-dependent response. Notably, this linear relationship closely matched that observed in fixed astrocyte cells heated using a stage-top incubator, suggesting that NIR laser stimulation has a similar heating function. Furthermore, the advantages of NIR laser stimulation go far beyond this. A recent study showed that 810 nm photobiomodulation significantly enhances calcium activity in both α- and β-cells.[27] Additionally, the temperature rapidly decreases once the laser

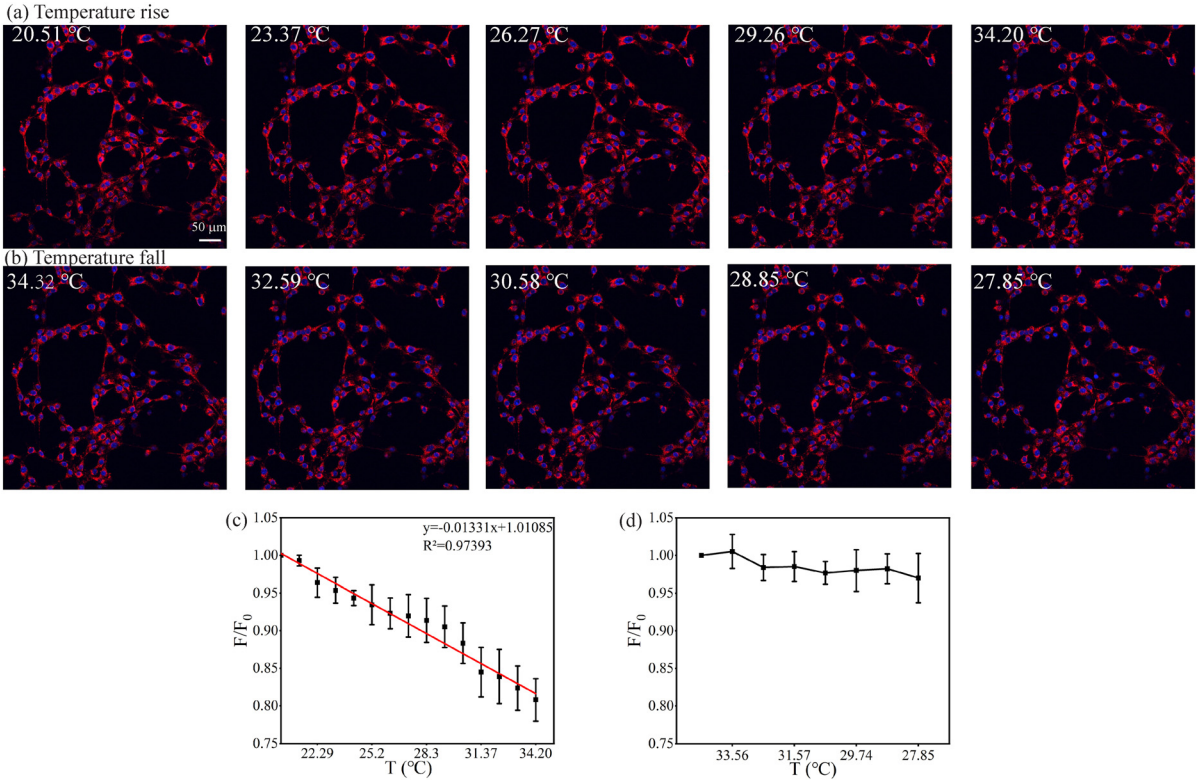

Fig. 4 Tracking changes in MTY fluorescence intensity through temperature changes in living astrocyte cells. (a) Time-lapse of MTY fluorescence intensity in astrocyte cells with increasing temperature. (b) Time-lapse of MTY fluorescence intensity in astrocyte cells with decreasing temperature. (c) Plot of MTY fluorescence intensity against increasing temperature in astrocyte cells. (d) Plot of MTY fluorescence intensity against decreasing temperature in astrocyte cells. Nuclei were counterstained with DAPI (blue) and imaged using a 20× objective lens.

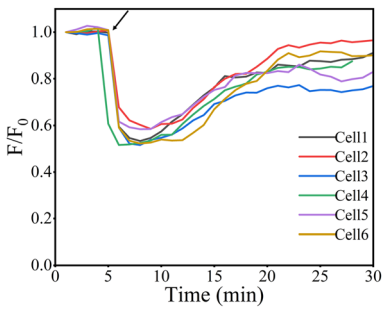

Fig. 5 Time-dependent changes in MTY fluorescence intensity within live astrocyte cells pre- and post-treatment with 10 μM FCCP. Mean fluorescence intensity (mean ± SD) from fluorescent cellular regions was quantified over time (n = 6 cells). Confocal images were acquired at 60 second intervals. Stained cells were exposed to 10 μM FCCP at the indicated time point (arrow).

is turned off, which helps minimize potential cell morphological changes.

3.8 Simultaneously tracking changes of mitochondrial-temperature sensitivity and calcium dynamics in living cells

We then utilized a spinning-disk confocal microscope to obtain simultaneous imaging of changes in intracellular temperature and calcium spikes that was accomplished using the green fluorescent calcium indicator Fluo-4 AM and the red fluorescent temperature-sensitive probe MTY. As shown in Fig. 7, when cells were exposed to elevated temperatures, the MTY fluorescence intensity gradually decreased, indicating a rapid rise in mitochondrial temperature. Meanwhile, the Fluo-4 AM fluorescence intensity also underwent changes, suggesting that intracellular calcium signaling was affected by temperature variations.

Furthermore, we also compared the Ca^{2+} oscillations under different conditions. As illustrated in Fig. S7, the traces show changes in fluorescence intensity ($\Delta F/F_0$) of Fluo-4 AM in live astrocyte cells under different situations. Under normal conditions, the cultured astrocytes exhibited infrequent (2–3 events per 10 minutes) and low-amplitude (<0.5 $\Delta F/F_0$) spontaneous Ca^{2+} oscillations. Therefore, a threshold of 0.5 $\Delta F/F_0$ was established to identify Ca^{2+} oscillations, with active Ca^{2+} spikes defined as those exceeding this threshold. Notably, Ca^{2+} oscillations increased significantly following 5-minute laser stimulation at 1064 nm. Similarly, Ca^{2+} oscillations were enhanced during heating using a stage-top incubator but gradually diminished, likely due to prolonged exposure to elevated temperatures. It was also revealed that synchronized mitochondrial thermogenesis and calcium transients, with thermal/laser stimulation inducing 2–4-fold greater calcium spiking *versus* controls.

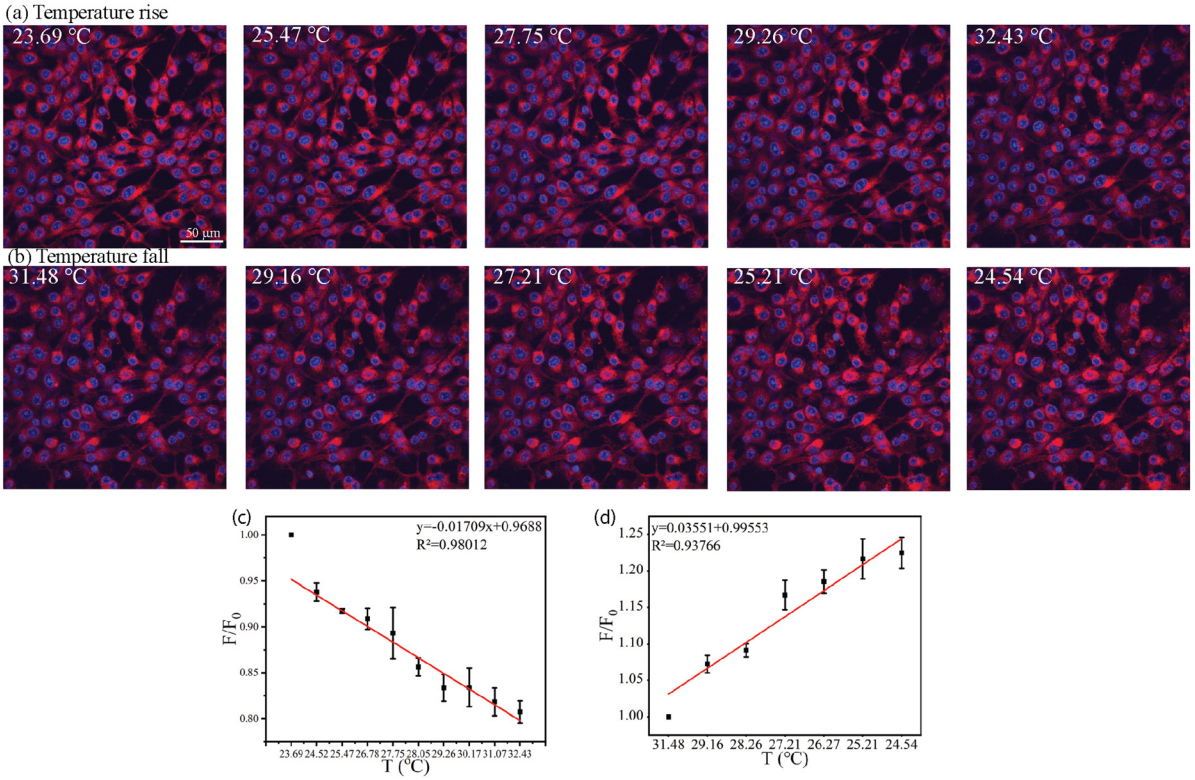

Fig. 6 Tracking changes in MTY fluorescence intensity under laser stimulation in living astrocyte cells. (a) Time-lapse of MTY fluorescence intensity in astrocyte cells with increasing temperature. (b) Time-lapse of MTY fluorescence intensity in astrocyte cells with decreasing temperature. (c) Plot of MTY fluorescence intensity against increasing temperature in astrocyte cells. (d) Plot of MTY fluorescence intensity against decreasing temperature in astrocyte cells. Nuclei were counterstained with DAPI (blue) and imaged using a 40× objective lens.

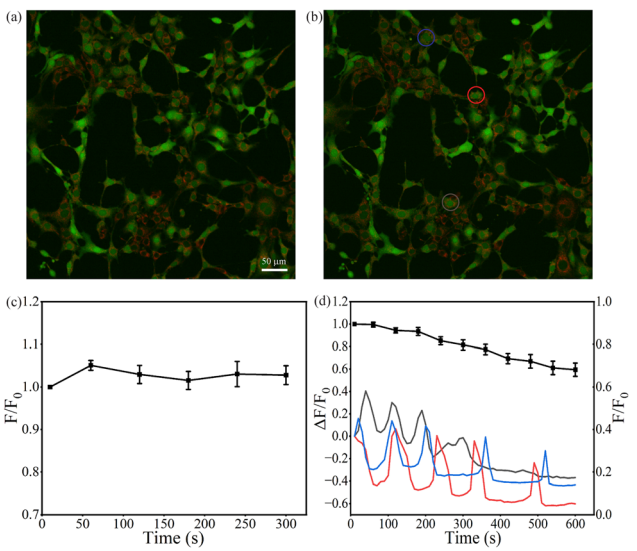

Fig. 7 Simultaneous tracking of changes in MTY (red color) and Fluo 4-AM (green color) fluorescence intensity through temperature changes in living astrocyte cells. (a and b) Time-lapse of MTY fluorescence intensity in astrocyte cells before and after increasing temperature. (c) Plot of MTY fluorescence intensity against room temperature in astrocyte cells. (d) Plot of MTY and Fluo 4-AM fluorescence intensity against increasing temperature in astrocyte cells. (The calcium dynamics of the three curves represent three individual cells circled in (b) under the same conditions.)

3.9 Assessing potential entry mechanism

Astrocytes, known as electrically non-excitable glial cells, exhibit Ca^{2+} fluctuations. These Ca^{2+} signals have the potential to propagate between glial cells *via* gap junctions.[28] To date, numerous studies have shown that astrocytic Ca^{2+} signalling arises from both intracellular stores and extracellular influx. Elevated cytosolic Ca^{2+} levels ($[Ca^{2+}]i$) in astrocytes result from two primary mechanisms: (1) transmembrane entry of extracellular Ca^{2+} through ion channels and (2) release of Ca^{2+} from the cytoplasmic reservoirs.[13] Extracellular Ca^{2+} influx occurs *via* channels such as the transient receptor potential (TRP) superfamily—including TRP vanilloid 4 (TRPV4) and TRP ankyrin 1 (TRPA1)—and voltage-gated calcium channels (VGCCs), all expressed in astrocytes.[29,30] Intracellular Ca^{2+} levels depend on triggered release of Ca^{2+} stored in the mitochondria or endoplasmic reticulum (ER); this release process is primarily mediated by inositol 1,4,5-trisphosphate (IP3) receptors, activated either by elevated $[Ca^{2+}]i$ or through metabotropic G-protein coupled receptor (GPCR) signalling at the plasma membrane or by the ryanodine receptor (RyR) located on the astrocytic ER.[30]

As for the NIR stimulation, Benfenati *et al.* utilized pulsed infrared light to modulate astrocyte function by altering $[Ca^{2+}]i$ and water dynamics. Their findings revealed that water transport is activated, with IP3R, TRPA1, TRPV4, and aquaporin-4 all playing roles in shaping the dynamics of infrared pulse-

evoked [Ca^{2+}]i signals.[31] Similarly, Albert *et al.* used mid-IR light (1875 nm laser) to irradiate retinal and vestibular ganglion cells, demonstrating that neuronal responses are mediated by TRPV4 channels.[32] These results demonstrate that astrocyte function can be modulated with infrared light.

Originally identified as a thermosensitive TRP channel, TRPV4 was later characterized as a thermosensor activated by temperatures between 27 and 34 °C.[33,34] Early studies by Liedtke *et al.* demonstrated that TRPV4 is responsive to warmer temperatures,[35] while Tominaga *et al.* revealed its role in mediating temperature-dependent microglial migration.[36] Beyond thermosensation, TRPV4 is thought to operate as a Ca^{2+} permeable nonselective cation channel, capable of being activated by a range of physical stimuli such as moderate heat (>27 °C), acidic conditions, osmotic changes, and mechanical stress.[37] Atrocytic TRPV4 has been implicated in several Ca^{2+}-dependent processes during the ischemic cascade, including excitotoxicity, oxidative stress, and astrocytic swelling.[38] Given its role in ischemia-related pathways, astrocytic TRPV4 is a potential compelling therapeutic target for brain ischemia. These findings motivated us to investigate the role of TRPV4 and its relationship with calcium dynamics when the temperature changes. Immunofluorescence staining confirmed the existence of TRPV4 in astrocytes, as shown in Fig. S8. We then investigated whether temperature elevation increases [Ca^{2+}]i in astrocytes through TRPV4 channels by monitoring calcium fluorescence using flow cytometry. The study was divided into two parts: inhibitor experiments and agonist experiments. For the inhibitor studies, four groups were compared: a room temperature (RT, 20 °C) control, an RT group treated with the TRPV4 inhibitor HC-067047, a high temperature (HT, 37 °C) group, and a HT group with HC-067047 treatment. HC-067047, a specific TRPV4 antagonist, effectively inhibited TRPV4 channel activity and partially blocked temperature-induced extracellular calcium ([Ca^{2+}]e) influx. As shown in Fig. S9, the control and HC-067047 (RT) groups exhibited nearly identical mean values, confirming that TRPV4 channels remain largely inactive at RT which is in agreement with prior findings[33,34] and that HC-067047 has negligible effects on baseline calcium levels. In contrast, the HT group exhibited a marked increase in fluorescence intensity compared to both RT groups, indicating that elevated temperature activates TRPV4 channels and enhances [Ca^{2+}]e influx. Importantly, this thermal response was significantly suppressed by HC-067047, as demonstrated by the reduced fluorescence in the HT + HC-067047 group, confirming the possibility of the inhibitor's ability to block TRPV4-mediated calcium signaling upon heat stimulation. In the agonist experiments, three groups were included: a RT control group, a 4α-PDD treatment group, and a 4α-PDD treatment with HT group. 4α-PDD, a TRPV4 channel agonist, activates TRPV4 channels by binding to them, leading to calcium influx. The results revealed that the fluorescence intensity in the 4α-PDD treatment group was significantly higher than that in the RT control group, confirming that 4α-PDD activates TRPV4 channels and increases [Ca^{2+}]e. Notably, the fluorescence intensity in the 4α-PDD treatment with HT group was higher than that in the 4α-PDD treatment group alone. This may be attributed to the intrinsic temperature sensitivity of TRPV4 channels, which can be activated by elevated temperature. The combined effect of 4α-PDD and temperature elevation synergistically enhanced TRPV4 channel activity, resulting in increasing [Ca^{2+}]e.

4 Conclusions

In this study, *in vitro* intracellular mitochondrial temperature determination and imaging have been performed using the fluorescent thermometer probe MTY. We systematically measured the intracellular temperature changes by changing the solution temperature reversibly in fixable, living and laser stimulated astrocyte cells. The methodology's adaptability was further demonstrated in additional cell lines, including MCF-7 and Panc02. A spinning-disk confocal microscope was utilized to achieve simultaneous imaging of mitochondrial temperature shifts and calcium spikes, the latter of which reflect neural activity. The elevation of the temperature or laser stimulation increased the calcium spikes of astrocyte cells remarkably in comparison with control cells, which possibly contributed to the extracellular Ca^{2+} influx *via* TRPV4 channels or triggered the release of Ca^{2+} stored in the mitochondria or ER. Further work focused on the exploitation of a more specific stimulation mechanism of this system and novel fluorescent probes to form intracellular targeted mitochondrial nanothermometers and their application is underway. These findings establish mitochondrial temperature as a vital factor for evaluating tissue health and metabolic activity. Real-time monitoring of mitochondrial thermal fluctuations could enhance our understanding of how temperature influences cellular behaviour and provide diagnostic insights into disorders tied to mitochondrial dysfunction. Such advances may ultimately catalyse novel strategies to detect and intervene in pathologies driven by metabolic dysregulation.

Abbreviations

NIR	Near-infrared
MTY	Mito Thermo Yellow
PKMDR	PKmito DEEP Red
4α-PDD	4α-Phorbol-12,13-didecanoate
CCK-8	Cell Counting Kit-8
TRPV4	Transient receptor potential vanilloid 4
ER	Endoplasmic reticulum
IP3	Inositol 1,4,5-trisphosphate
VGCCs	Voltage-gated calcium channels
FCCP	Carbonyl cyanide 4-(trifluoromethoxy) phenylhydrazone

Author contributions

M. N. Sun, A. G. Wu and B. Chen conceived and planned the experiments. M. N. Sun investigated and analyzed the experi-

mental data. B. Chen wrote and finalized the original manuscript. B. Chen and A. G. Wu supervised this work. A. G. Wu provided an insightful suggestion for revision. All authors reviewed and commented on the manuscript.

Conflicts of interest

There are no conflicts to declare.

Data availability

The data supporting this article have been included as part of the Supplementary Information (SI). The SI includes an expanded experimental section, details on a custom-built NIR laser imaging system, fluorescence data for MTY under various conditions (room temperature, thermal changes, and FCCP treatment), optimization of NIR laser parameters, analysis of astrocyte calcium dynamics, an assessment of the cellular entry mechanism, and supplementary figures. See DOI: **https://doi.org/10.1039/d5bm00691k**.

Acknowledgements

This research was supported by the Zhejiang Provincial Basic Public Welfare Research Foundation of China under Grant No. LGC22B030003 and the Ningbo Yongjiang Talent Introduction Program of China under Grant No. 2021A-088-G. We thank all the staff of the Instrumental Testing Center for imaging assistance and insightful discussions.

References

1 G. J. Tattersall, B. J. Sinclair, P. C. Withers, P. A. Fields, F. Seebacher, C. E. Cooper and S. K. Maloney, *Compr. Physiol.*, 2012, **2**, 2151–2202.
2 P. Wendering and Z. Nikoloski, *Biotechnol. Adv.*, 2023, **67**, 108203.
3 A. N. Mugo, R. Chou and F. Qin, *Proc. Natl. Acad. Sci. U. S. A.*, 2025, **122**, e2406318121.
4 J. Chen, V. Nolte and C. Schlötterer, *Mol. Biol. Evol.*, 2015, **32**, 2393–2402.
5 C. Desler and L. J. Rasmussen, *Mitochondrion*, 2014, **16**, 2–6.
6 A. M. Bertholet and Y. Kirichok, *Annu. Rev. Physiol.*, 2022, **84**, 381–407.
7 R. Howard, A. Scheiner, J. Cunningham and R. Gatenby, *PLoS Comput. Biol.*, 2019, **15**, e1007372.
8 Z. Huang, N. Li, X. Zhang and Y. Xiao, *Anal. Chem.*, 2021, **93**, 5081–5088.
9 D. Chretien, P. Bénit, H. H. Ha, S. Keipert, R. El-Khoury, Y. T. Chang, M. Jastroch, H. T. Jacobs, P. Rustin and M. Rak, *PLoS Biol.*, 2018, **16**, e2003992.
10 B. S. Khakh and M. V. Sofroniew, *Nat. Neurosci.*, 2015, **18**, 942–952.
11 J. T. Weber, *Curr. Neurovasc. Res.*, 2004, **1**, 151–171.
12 M. J. Berridge, M. D. Bootman and H. L. Roderick, *Nat. Rev. Mol. Cell Biol.*, 2003, **4**, 517–529.
13 J. Goenaga, A. Araque, P. Kofuji and D. Herrera Moro Chao, *Front. Synaptic Neurosci.*, 2023, **15**, 1138577.
14 G. Szabadkai and M. R. Duchen, *Physiology*, 2008, **23**, 84–94.
15 J. Ma, R. Sun, K. Xia, Q. Xia, Y. Liu and X. Zhang, *Chem. Rev.*, 2024, **124**, 1738–1861.
16 J. Zhou, B. Del Rosal, D. Jaque, S. Uchiyama and D. Jin, *Nat. Methods*, 2020, **17**, 967–980.
17 D. Jaque, B. D. Rosal, E. M. Rodríguez, L. M. Maestro, P. Haro-Gonzalez and J. G. Solé, *Nanomedicine*, 2014, **9**, 1047–1062.
18 S. Arai, M. Suzuki, S. J. Park, J. S. Yoo, L. Wang, N. Y. Kang, H. H. Ha and Y. T. Chang, *Chem. Commun.*, 2015, **51**, 8044–8047.
19 Q. Zhu, Y. Sun, M. Fu, M. Bian, X. Zhu, K. Wang, H. Geng, W. Zeng, W. Shen and Y. Hu, *ACS Sens.*, 2022, **8**, 51–60.
20 M. Homma, Y. Takei, A. Murata, T. Inoue and S. Takeoka, *Chem. Commun.*, 2015, **51**, 6194–6197.
21 Z. Huang, N. Li, X. Zhang, C. Wang and Y. Xiao, *Anal. Chem.*, 2018, **90**, 13953–13959.
22 F. Shen, W. Yang, J. Cui, Y. Hou and G. Bai, *Anal. Chem.*, 2021, **93**, 13417–13420.
23 T. Liu, T. Stephan, P. Chen, J. Keller-Findeisen, J. Chen, D. Riedel, Z. Yang, S. Jakobs and Z. Chen, *Proc. Natl. Acad. Sci. U. S. A.*, 2022, **119**, e2215799119.
24 K. Neikirk, A. G. Marshall, B. Kula, N. Smith, S. LeBlanc and A. Hinton Jr, *Eur. J. Cell Biol.*, 2023, **102**, 151371.
25 A. C. Cutró, G. G. Montich and O. A. Roveri, *J. Bioenerg. Biomembr.*, 2014, **46**, 119–125.
26 Z. Fekete, Á. C. Horváth and A. Zátonyi, *J. Neural Eng.*, 2020, **17**, 051003.
27 C. Liebman, S. Loya, M. Lawrence, N. Bashoo and M. Cho, *J. Biophotonics*, 2022, **15**, e202100257.
28 N. Bazargani and D. Attwell, *Nat. Neurosci.*, 2016, **19**, 182–189.
29 Y. Bai, Z. Zhou, B. Han, X. Xiang, W. Huang and H. Yao, *Fundam. Res.*, 2024, **4**, 1365–1374.
30 E. Shigetomi, S. Patel and B. S. Khakh, *Trends Cell Biol.*, 2016, **26**, 300–312.
31 A. I. Borrachero-Conejo, W. R. Adams, E. Saracino, M. G. Mola, M. Wang, T. Posati, F. Formaggio, M. De Bellis, A. Frigeri and M. Caprini, *FASEB J.*, 2020, **34**, 6539–6553.
32 E. Albert, J. M. Bec, G. Desmadryl, K. Chekroud, C. Travo, S. Gaboyard, F. Bardin, I. Marc, M. Dumas and G. Lenaers, *J. Neurophysiol.*, 2012, **107**, 3227–3234.
33 H. Watanabe, J. Vriens, S. H. Suh, C. D. Benham, G. Droogmans and B. Nilius, *J. Biol. Chem.*, 2022, **277**, 47044–47051.
34 A. D. Güler, H. Lee, T. Iida, I. Shimizu, M. Tominaga and M. Caterina, *J. Neurosci.*, 2002, **22**, 6408–6414.

35 W. Liedtke, Y. Choe, M. A. Martí-Renom, A. M. Bell, C. S. Denis, A. J. Hudspeth, J. M. Friedman and S. Heller, *Cell*, 2000, **103**, 525–535.
36 R. Nishimoto, S. Derouiche, K. Eto, A. Deveci, M. Kashio, Y. Kimori, Y. Matsuoka, H. Morimatsu, J. Nabekura and M. Tominaga, *Proc. Natl. Acad. Sci. U. S. A.*, 2021, **118**, e2012894118, DOI: **10.1073/pnas.2012894118**.
37 T. K. Acharya, A. Kumar, R. K. Majhi, S. Kumar, R. Chakraborty, A. Tiwari, K. H. Smalla, X. Liu, Y. T. Chang and E. D. Gundelfinger, *Mitochondrion*, 2022, **67**, 38–58.
38 J. Tureckova, Z. Hermanova, V. Marchetti and M. Anderova, *Int. J. Mol. Sci.*, 2023, **24**, 7101, DOI: **10.3390/ijms24087101**.